NUREG/CR-6780

Effects of Adsorption Constant Uncertainty on Contaminant Plume Migration: One- and Two-Dimensional Numerical Studies

Manuscript Completed: April 2002
Date Published: May 2002

Prepared by
Louise J. Criscenti[1], Mehdi Eliassi[2], Randall T. Cygan[1], and Carlos F. Jové Colón[3]

Sandia National Laboratories
Albuquerque, NM 87185-0750 USA

E. O'Donnell, NRC Project Manager

Prepared for
US Nuclear Regulatory Commission
Office of Nuclear Regulatory Research
Division of Risk Analysis and Applications
Radiation Protection, Environmental Risk and Waste Management Branch
MS T9-F31
Washington, DC 20555-0001
NRC Job Code W6811

[1] Geochemistry Department, Sandia National Laboratories, Albuquerque, NM 87185-0750
[2] Geohydrology Department, Sandia National Laboratories, Albuquerque, NM 87185-0735
[3] Total Systems Performance Assessment Department, Sandia National Laboratories, Albuquerque, NM 87185-0778

Abstract

In this study, one- and two-dimensional (1-D and 2-D) reactive-transport models, with specific application to the hydrology and mineralogy of the Naturita uranium mill tailings site in Colorado, are used to examine variations in model predictions due to uncertainty in the model adsorption constants. This work demonstrates the importance of selecting the appropriate adsorption constants when using reactive-transport models to evaluate risk and pollution attenuation at contaminated sites. In our models, uranium is removed from uranium mill tailings leachate through adsorption onto smectite, an abundant clay mineral at the Naturita site. Uranium adsorbs to specific surface sites on both the basal planes and edges of the smectite. Because uranium adsorbs predominantly to the aluminum edge surface sites [>(e)AlOH], uncertainty was examined only in the equilibrium constants associated with these sites. One hundred pairs of equilibrium constant (log K) values for the surface species >(e)AlO^- and >(e)$AlOUO_2^+$ were selected from normal distributions of each log K using the Latin Hypercube Sampling method. For the 1-D simulations, two distinct groups of uranium breakthrough curves can be identified. In the first group, the breakthrough curves exhibited a classical sigmoidal shape whereas in the second group the breakthrough curves displayed higher uranium concentrations in solution over greater distances and times. These two groups are clearly separated by two different ranges of log K >(e)AlO^- values or two different ranges for the smectite point of zero charge. Preliminary 2-D simulations also demonstrate that predictions of both transverse and longitudinal plume migration are influenced by the choice of adsorption constants.

Contents

Figures

Tables

Acknowledgments

The authors would like to acknowledge the insightful discussions with Craig Bethke, Gary Curtis, James Davis, Edward O'Donnell, and Henry Westrich that helped during the course of the research. Edward O'Donnell, Ralph Cady, John Randall, Henry Westrich, and Jon Helton provided valuable reviews of the original manuscript that greatly benefited the final paper. This work was supported by the Nuclear Regulatory Commission, Office of Nuclear Regulatory Research. The authors are very grateful for the advice and support provided by NRC program manager Edward O'Donnell during the funding period. Sandia National Laboratories is a multi-program laboratory operated by the Sandia Corporation, a Lockheed Martin Company, for the United States Department of Energy under Contract DE-AC04-94AL85000.

Page intentionally left blank.

1. INTRODUCTION

This study builds upon recent investigations of uranium mill tailings sites where uranium [U(VI)] has leached into the surrounding soil for many years (e.g., Morrison and Cahn, 1991; Landa and Gray, 1995; Zhu and Burden, 2001; Zhu et al., 2001; Bain et al., 2001). One site under investigation is Naturita, Colorado, where the Nuclear Regulatory Commission is working cooperatively with the U. S. Geological Survey and Sandia National Laboratories to investigate both hydrological and geochemical conditions as a function of time and assess the ability of surface complexation models coupled with hydrologic models to predict radionuclide migration through the soil (Davis, 2001; Davis et al., 2001; Curtis et al., 2001, 2002; Jové Colón et al., 2001; Jacobs Engineering Group Inc., 1994). Naturita is one of several Uranium Mill Tailings Remedial Action (UMTRA) Title 1 sites where the mine tailings have been removed by the U.S. Government to reduce contaminant levels. However, lingering uranium dissolved in groundwater and adsorbed in shallow alluvium still remains, creating some concerns regarding the extent of contaminant transport within the site. In this study, coupled reactive-transport models are used to better conceptualize and predict uranium migration at the contamination sites, with particular application to the hydrology and mineralogy associated with Naturita. This work demonstrates the importance of selecting the appropriate adsorption constants when using reactive-transport models to evaluate pollutant attenuation and potential risk at contaminated sites.

The issue of uncertainty analysis and its importance when using various models to describe contaminant migration in the subsurface environment is not a new one. Several studies have investigated uncertainty in geochemical modeling (Criscenti et al., 1996; Stipp et al., 1990; Schecher and Driscoll, 1987, 1988; Nordstrom and Ball, 1989; Anderson, 1976). While reactive-transport modeling has also been used in the past to investigate the migration of uranium in mill tailings, such studies have primarily focused on examining the development of reaction fronts due to mineral precipitation and dissolution (Zhu and Burden, 2001; Zhu et al., 2001; Bain et al., 2001; Erikson et al., 1990). Several studies have also examined the sensitivity of reactive-transport simulations to uncertainty in hydrological parameters (e.g., Hamed et al., 1996; Nietzsche et al., 2000).

More recently, Tebes-Stevens and Valocchi (2000) and Tebes-Stevens et al. (2001) have studied the relative effects of transport and reaction parameters on the results of a solute transport model. Uranium(VI) hydrolysis species are transported through a 2-D domain with a spatially variable pattern of surface complexation sites (Tebes-Stevens et al., 2001). Using a non-electrostatic surface complexation model, their calculations indicated that the model is most sensitive to the initial concentration of one of two types of surface sites, the formation constant for one of three uranyl (UO_2^{2+}) surface complexes, and the hydraulic conductivity within the reactive zone.

To investigate the effects of uncertainty in two equilibrium adsorption constants in an electrostatic surface complexation model, simple 1-D and 2-D reactive-transport models were applied. The investigation focused on examining uranium adsorption onto clay surfaces, one of several possible retardation mechanisms at the Naturita site, and the influence of the adsorption constants on calculated uranium breakthrough curves and migration. Adsorption onto other solid phases, such as ferrihydrite, has also been suggested at the Naturita site (Davis et al., 2001). In addition, ongoing analytical research suggests that uranium contamination at the Naturita site is strongly affiliated with iron-rich coatings (Jové Colón et al., 2002). However, for the uncertainty analysis presented here, the adsorption model used includes a total of two active adsorption sites for uranyl onto both the basal and surface edges of smectite clay. The results suggest that uncertainties in these parameters can lead to widely differing predictions of uranium migration in the subsurface environment that could pose a problem when addressing the risk associated with contaminant migration from mill tailings.

2. GOVERNING EQUATIONS

The advective-dispersive-reactive (ADR) transport model in a 2-D system was considered to evaluate the flow conditions for the reactive-transport system. Under water-saturated conditions, of interest in this work, the governing equation for ADR, described in 2-D tensor notation, can be stated as (Bethke 1997a):

$$\phi\frac{\partial C_i}{\partial t}=\frac{\partial}{\partial x_l}\left(\phi D_{lm}\frac{\partial C_i}{\partial x_m}\right)-\frac{\partial}{\partial x_l}(q_l C_i) -\phi\sum_k\left(\frac{\partial C_i}{\partial t}\right)_k+\phi Q_i \quad (1)$$

where ϕ is the porosity, C_i [M/L^3] is the concentration of the transport component, i, t [T] is time, x_l=(x,y) [L] represents the cartesian coordinates, D_{lm} [L^2/T] is the dispersion tensor, q_l [L/T] is the specific discharge, subscripts m and l refer to the spatial directions, the term involving the summation over k refers to the mass transfer among the various transport species, and Q_i [M/TL^3] is a source/sink term. In a 2-D system, the components for the dispersion tensor may be defined as (Bear and Verruijt, 1987):

$$D_{xx}=\alpha_T\bar{v}+(\alpha_L-\alpha_T)\frac{v_x^2}{\bar{v}}+D_0 \quad (2a)$$

$$D_{yy}=\alpha_T\bar{v}+(\alpha_L-\alpha_T)\frac{v_y^2}{\bar{v}}+D_0 \quad (2b)$$

$$D_{xy}=D_{yx}=(\alpha_L-\alpha_T)\frac{v_x v_y}{\bar{v}} \quad (2c)$$

where D_{xx} and D_{yy} [L^2/T] are the dispersion coefficients along the main diagonal, D_{xy} and D_{yx} [L^2/T] are off-diagonal dispersion coefficients, α_T [L] and α_L [L] are respectively the transverse and longitudinal dispersivities, v_x and v_y [L/T] are the pore velocities in the x- and y-directions, respectively, $\bar{v}$ [L/T] is the average velocity, and D_0 [L^2/T] is the coefficient of molecular diffusion assumed to be 10^{-6} m^2/sec throughout this work. Additionally, α_L and α_T are considered constant and independent of direction. In addition, α_L is 1% of the domain length (i.e., in the x-direction) and α_T=α_L/10, which is found to be reasonable under measured field conditions (e.g., see Gelhar, 1986; Neuman, 1990; Domencio and Schwartz, 1990).

2.1 Governing Geochemical Equations

The geochemical composition of each species in the system (e.g., aqueous, surface, solid phase) is usually described in terms of chemical components. Each independent reaction that forms an aqueous species in the system has an associated equilibrium constant K_j at the temperature of interest and therefore can be described by a mass action equation. Under the equilibrium state (Bethke, 1996):

$$m_j=\frac{1}{K_j\gamma_j}\left(a_w^{\nu_{wj}}\prod_i(\gamma_i m_i)^{\nu_{ij}}\prod_k a_k^{\nu_{kj}}\prod_m f_m^{\nu_{mj}}\right) \quad (3)$$

where a_w is the water activity, γ_i and γ_j are the activity coefficients for the component i and aqueous species j, m_i and m_j are the molalities of the component i and species j, a_k is the activity of the mineral k, f_m is the fugacity of gas m, and ν_{ij}, ν_{kj}, and ν_{mj} are the stoichiometric coefficients of the components, solid phases, and gas fugacities, respectively, in reactions to form aqueous species j.

Similar equations can also be written for each surface species within the framework of a surface complexation model, such as the diffuse-layer model (DLM) of Dzombak and Morel (1990). However, in addition to considering the chemical contributions to the free energy change of reaction, the electrostatic work involved in moving each ion through the electric potential field created by the mineral surface needs to be considered. Therefore, the mass action equations for the DLM surface complexes have the following form (Bethke, 1996):

$$m_q=\frac{1}{K_q 10^{z_q F\Psi/2.303RT}}\left(a_w^{\nu_{wq}}\prod_i(\gamma_i m_i)^{\nu_{iq}}\prod_k a_k^{\nu_{kq}}\prod_m f_m^{\nu_{mq}}\prod_p m_p^{\nu_{pq}}\right) \quad (4)$$

where z_q is the electrical charge on each complex q, F [96,485 C/mol] is the Faraday constant, Ψ [V] is the surface potential, R [8.3143 V·C/mol·K where 1 V·C = 1 Joule] is the gas constant, T [K] is absolute temperature, m_p and m_q are the molalities of the uncomplexed and complexed surface sites, respectively, and ν_{wq}, ν_{iq},

v_{kq}, v_{mq}, and v_{pq} are coefficients in the reaction for surface complex q.

Mass balance equations that express the conservation of mass in terms of mole number for water (M_w), each component (M_i), mineral (M_k), gas (M_m), and site type (M_p) are stated as (Bethke, 1998):

$$M_w = n_w\left(55.5 + \sum_j v_{wj} m_j + \sum_q v_{wq} m_q\right) \quad (5a)$$

$$M_i = n_w\left(m_i + \sum_j v_{ij} m_{ij} + \sum_q v_{iq} m_q\right) \quad (5b)$$

$$M_k = n_k + n_w\left(\sum_j v_{kj} m_j + \sum_q v_{kq} m_q\right) \quad (5c)$$

$$M_m = n_w\left(\sum_j v_{mj} m_j + \sum_q v_{mq} m_q\right) \quad (5d)$$

$$M_p = n_w\left(m_p + \sum_q v_{pq} m_q\right) \quad (5e)$$

where n_w is the mass of solvent water. These relationships form a set of governing equations describing multicomponent equilibrium in the presence of an adsorbing mineral surface.

The principle of electroneutrality requires that the ionic species in aqueous solution remain charge balanced on a macroscopic scale. This requirement is met in X1t and X2t by adjusting M_i for one component. By default, this component is chloride (Cl^-) because it is in abundant concentration and because most commercial laboratories report a chloride concentration calculated by a rough charge balance (Bethke, 1996). In this study, either Cl^- or SO_4^{2-} another major anion in uranium mill-tailings leachate is used as the charge-balancing anion.

2.2 Numerical Solution of Coupled Reactive Transport Equations

To numerically solve the system of equations (1) through (5), the X1t and X2t software codes are used for 1-D and 2-D simulations, respectively (Bethke, 1997a, b). In the Xt package, the spatial derivatives of transport equations are discretized based on the cell-centered finite difference method. Additionally, Xt uses the Strang operator splitting approach to advance the time step, where the flow equation is first solved to arrive at the nodal hydraulic potential values, and thus computes the specific discharge between two neighboring nodes. Next, the ADR equations are solved using explicit time stepping, where the spatial averaging across cell boundaries is performed by first-order upwind weighting. Note that to ensure numerical stability, Xt also calculates the time-step size based on a combination of the Courant condition for the advective and von Neumann's criterion for the dispersive components of the transport equations.

The numerical solution for the geochemical model of the coupled reactive-transport codes, X1t and X2t, has been described by Bethke (1996, 1998). To summarize, at each time step, equilibrium speciation and partitioning between the solid matrix, mineral surfaces, and aqueous solution are calculated based on the mass action and mass balance equations. The resulting system of algebraic, nonlinear equations is then solved using the Newton-Raphson method (Bethke, 1996). The aqueous solution is checked for charge balance and adjusted by adding or subtracting mass from the charge-balancing component. These two steps, solving the system of nonlinear equations and correcting the solution charge balance, are repeated until the chemistry converges to within a predefined level of tolerance. The surface complexation model available in the Xt codes is the diffuse layer model (DLM) of Dzombak and Morel (1990) that describes the mineral/water interface in terms of a surface layer and a diffuse layer. During each simulation time step, as the fluid enters and leaves the finite-difference cell, each cell is reequilibrated based on the new solution composition.

3. GEOCHEMICAL MODEL

Because of the interest in the Naturita field site, both 1-D and 2-D conceptual models were developed that mainly focused on uranium migration in the subsurface environment. In these models, the initial system consists of an aqueous solution that is in equilibrium with a clay mineral comprised of basal and edge surfaces (see Table 1); it is assumed there is no interlayer exchange with uranium. This equilibrium system is buffered by CO_2 and O_2 reservoirs representative of an aquifer environment.

In the 1-D conceptual model, leachate from the uranium mill tailings is assumed to have already saturated the subsurface porous system with uranium. Therefore, uranium is initially distributed homogeneously in the subsurface. The initial groundwater composition (see Table 2) reflects prior mixing with uranium mill tailings leachate; it contains much higher concentrations of SO_4^{2-} (1500 mg/kg), Cl^- (84.4 mg/kg), Na^+ (226 mg/kg), Ca^{2+} (209.0 mg/kg), and Mg^{2+} (60.5 mg/kg) than are typically present in natural groundwater. This composition is representative of water samples collected downstream from the Naturita site in 1999 by the U. S. Geological Survey (Kohler et al., 2001; Davis et al., 2001). The inlet rainwater composition is that reported by Berner and Berner (1987) for precipitation in the inland western United States. The mixing of the rainwater with contaminated groundwater was examined in the 1-D model, similar to what is occurring at Naturita today. The 2-D conceptual model examines a somewhat different application, where contaminant is leached from a point source into the uncontaminated groundwater. This scenario is representative of the processes associated with the initial development of a uranium groundwater plume. For this second model, the initial groundwater composition is characteristic of those reported at wells upstream from the uranium mill-tailings at the Naturita site. This groundwater composition is assumed to constantly flow through the domain. An injection well in the model represents a point source of contamination from which leachate with the composition of the currently contaminated groundwater at the Naturita site is injected into the system.

In order to investigate the effects of adsorption constant uncertainty on predictions of uranium migration, the soil in both the 1-D and 2-D conceptual models is represented simply by one clay mineral, a smectite. The precipitation and dissolution of other phases like hydrous ferric oxide and gypsum that might occur in this system are neglected. In addition, the model only considers uranium adsorption to one solid phase, although uranium may adsorb to several solid phases at the Naturita site, such as ferrihydrite. The mineral selected as a representative clay substrate is a low-Fe-Mg smectite, with a composition given by $Na_{0.15}Ca_{0.02}K_{.2}Mg_{0.9}Fe_{0.45}Al_{1.25}Si_{3.75}O_{10}$ $(OH)_2$, that forms according to the following fundamental reaction:

$$0.29\ Fe^{2+} + 0.16\ Fe^{3+} + 0.02\ Ca^{2+} + 0.2\ K^+ + 0.15\ Na^+ + 0.9\ Mg^{2+} + 1.25\ Al^{3+} + 3.75\ SiO_2(aq) + 4.5\ H_2O \leftrightarrow 7\ H^+ + Na_{0.15}Ca_{0.02}K_{.2}Mg_{0.9}Fe_{0.45}Al_{1.25}Si_{3.75}O_{10}(OH)_2 \quad (6)$$

with an association constant of $10^{-11.5537}$ (log K = -11.5537) at 25°C that is reported in the thermodynamic database contained in Geochemist's Workbench 3.0 (Bethke, 1998). Smectite is a layered sheet aluminosilicate containing thin platelets of alumina octahedra and silica tetrahedra coordinated to interlayer cations (i.e., Na^+, K^+, Ca^{2+}, Fe^{2+}, Fe^{3+}, and Mg^{2+}).

Recent molecular modeling of cesium adsorption on kaolinite (Cygan et al., 1998), a simpler clay mineral, suggests that cesium adsorbs directly to the Al octahedra on the (100), (010), and (110) surface edges of kaolinite and is coordinated to four aluminols to form a strong inner-sphere complex. Similar reactive surface sites are suggested for the smectite clays. Zachara and McKinley (1993) fit bulk data for uranyl adsorption onto smectite minerals using a computational model that includes fixed-charge sites and edge aluminum hydroxyls. A different surface complexation model, the triple-layer model (TLM) (Davis and Leckie, 1978, Davis et al., 1978), was applied to edge-site complexation. The uranyl adsorption data is consistent with a surface speciation scheme dominated by ion exchange and aluminol edge complexation ($>AlOUO_2^+$, where > indicates that the species is bound to the surface). Therefore, as a first approximation, it was assumed that the uranyl cation only binds to the Al surface sites of smectite.

Table 1. List of chemical species considered in geochemical model.

Components

H^+	Ca^{2+}	Cl^-	>(b) AlOH
Na^+	Fe^{2+}	NO_3^-	>(e) AlOH
K^+	Fe^{3+}	HCO_3^-	
Mg^{2+}	Al^{3+}	SO_4^{2-}	
SiO_2	UO_2^{2+}		

Aqueous Complexes

OH^-	$CaOH^+$	$FeOH^+$	$AlOH^{2+}$	$(UO_2)_2(OH)_2^{2+}$
	$CaCl^+$	$Fe(OH)_2$	$Al(OH)_2^+$	$(UO_2)_3(OH)_4^{2+}$
HCl	$CaHCO_3^+$	$Fe(OH)_3^-$	$Al(OH)_3$	$(UO_2)_3(OH)_5^+$
HSO_4^-	$CaCO_3$	$FeHCO_3^+$	$Al(OH)_4^-$	$(UO_2)_3(OH)_7^-$
	$CaSO_4$	$FeCO_3$	$Al_{13}O_4(OH)_{24}^{7+}$	$(UO_2)_4(OH)_7^+$
NaOH	$CaH_3SiO_4^+$	$FeCl^+$	$Al_2(OH)_2^{4+}$	UO_2SO_4
NaCl	CaH_2SiO_4	$FeCl_2$	$Al_3(OH)_4^{5+}$	$UO_2(SO_4)_2^{2-}$
$NaHCO_3$	$Ca(H_3SiO_4)_2$	$FeSO_4$	$AlSO_4^+$	$UO_2(NO_3)_2$
$NaSO_4^-$	$CaNO_3^+$		$Al(SO_4)_2^-$	$UO_2SiO(OH)_3^+$
$NaCO_3^-$				$(UO_2)^{2+}(CO_3)(OH)_3^-$
NaH_3SiO_4	$MgOH^+$	$FeOH^{2+}$	$H_3SiO_4^-$	UO_2CO_3
	Mg_2OH^{3+}	$Fe(OH)_2^+$	$H_2SiO_4^{2-}$	$UO_2(CO_3)_2^{2-}$
KOH	$Mg_4(OH)_4^{4+}$	$Fe(OH)_3$	$H_3SiO_4^-$	$UO_2(CO_3)_3^{3-}$
KCl	$MgCl^+$	$Fe(OH)_4^-$	$H_4(H_2SiO_4)_4^{4-}$	
KSO_4^-	$MgHCO_3^+$	$Fe_2(OH)_2^{4+}$	$H_6(H_2SiO_4)_4^{2-}$	
	$MgCO_3$	$Fe_3(OH)_4^{5+}$		
CO_3^{2-}	$Mg_2CO_3^{2+}$	$FeCO_3^+$		
CO_2(aq)	MgH_2SiO_4	$FeCl_2^+$		
	$MgH_3SiO_4^+$	$FeCl_4^-$		
	$Mg(H_3SiO_4)_2$	$FeCl_3$		
	$MgSO_4$	$FeH_3SiO_4^{2+}$		
		$FeSO_4^+$		
		$Fe(SO_4)_2^-$		
		$FeNO_3^{2+}$		

Solid Phase

Low-Fe-Mg Smectite

$Na_{.15}Ca_{.02}K_{.2}Mg_{.9}Fe_{.45}Al_{1.25}Si_{3.75}O_{10}(OH)_2$

Surface Complexes

>(e)AlO^-	>(e)$AlOH_2^+$	>(e)$AlOUO_2^+$
>(b)AlO^-	>(b)$AlOH_2^+$	>(b)$AlOUO_2^+$

Table 2. Initial groundwater, rainwater, and leachate compositions used in 1-D and 2-D simulations.

	1-D Simulations		2-D Simulations		
	Contaminated Groundwater	Rainwater	Initial Groundwater	Incoming Groundwater	Leachate
pH	7	5.8	7	7	**7**
fCO_2(g) (*atm*)	$10^{-2.5}$	$10^{-3.5}$	$10^{-2.5}$	$10^{-2.5}$	$10^{-2.5}$
fO_2(g) (*atm*)	0.2	0.2	0.2	0.2	0.2
Na^+ (*mg/kg*)	226	0.4	25	25	226
K^+ (*mg/kg*)	7.85	0.2	2	2	7.85
Mg^{2+} (*mg/kg*)	60.5	0.1	20	20	60.5
Ca^{2+} (*mg/kg*)	209.0	1.4	70	70	209.0
Fe^{2+} (*mg/kg*)	0.10	1×10^{-8}	0.10	0.10	0.10
Fe^{3+} (*mg/kg*)	0.01	1×10^{-8}	0.01	0.01	0.01
UO_2^{2+} (*mg/kg*)	3.14	1×10^{-32}	1×10^{-6}	1×10^{-6}	3
SiO_2 (aq) (*mg/kg*)	12	1×10^{-8}	10.7	10.7	12
Cl^- (*mg/kg*)	84.4 (809)[1]	0.41 (0.61)[1]	11	11	84.4 (68)
NO_3^- (*mg/kg*)	0.03	1.20	0.03	0.03	0.03
SO_4^{2-} (*mg/kg*)	1500	3.0	315 (1208)[1]	315 (260)[1]	1100
Al^{3+} (*mg/kg*)	0.013[2]	1×10^{-8}	0.013[2]	0.013	0.013

[1] () indicates concentration after charge balance. These new concentrations are well within the range reported at the Naturita site.

[2] Concentration of Al^{3+} that is in equilibrium with low-Fe-Mg smectite.

These surface sites are divided into two groups with different characteristics based on whether they occur on the basal planes or edges of smectite (Fig. 1). Following Pabalan et al. (1998), who developed a model for the adsorption of uranyl onto montmorillonite derived from experimental data, a total surface site density of approximately 2.3 sites/nm^2 that has been recommended by Davis and Kent (1990) for all minerals and by Dzombak and Morel (1990) for ferrihydrite was assumed.

Two different types of surface sites were used to fit metal adsorption data for ferrihydrite using the DLM (Dzombak and Morel, 1990). The high-affinity sites adsorb divalent metal cations more readily than the low-affinity sites. For ferrihydrite, the high-affinity surface sites are much less abundant (0.23 sites/nm^2) than the low-affinity sites. For low-Fe-Mg smectite, a higher site density was chosen for the surface sites on the platelet edges that have a higher affinity for cation adsorption (e.g., UO_2^{2+}) than for the sites on the basal plane (see Fig. 1). However, the edge surface area of a smectite is much smaller than that of the basal planes. For montmorillonite, Pabalan et al. (1998) assumed the effective edge surface area to be 10% of total N_2-BET surface area (97 m^2/g). Here, a similar total surface area (100 m^2/g) for smectite, and a similar distribution of surface area between the edges (i.e., 10 m^2/g) and basal planes (i.e., 90 m^2/g) was assumed (Brady et al., 1998; Schlegel et al., 1999).

The edge Al surface sites are amphoteric in nature and, depending on the pH of the solution, they can protonate and deprotonate to form charged surface sites. For example, a neutral Al edge surface site [$>(e)AlOH$] gains or loses a proton to create a positively-charged (z_q =1) or negatively-charged (z_q = -1) surface species, according to the following reactions within the context of the DLM:

$$>(e)AlOH + H^+ \leftrightarrow >(e)AlOH_2^+;$$
$$K = \frac{m_{>(e)AlOH_2^+}}{m_{>(e)AlOH}\, a_{H^+}} 10^{(+F\Psi/2.303RT)} \qquad (7a)$$

$$>(e)AlOH \leftrightarrow >(e)AlO^- + H^+;$$
$$K = \frac{m_{>(e)AlO^-}\, a_{H^+}}{m_{>(e)AlOH}} 10^{(-F\Psi/2.303RT)} \qquad (7b)$$

where all variables have been previously defined. Analogous equations can be written for protonation and deprotonation of the basal Al surface sites [$>(b)AlOH$], but experimental evidence suggests that only deprotonated sites exist on this surface for most

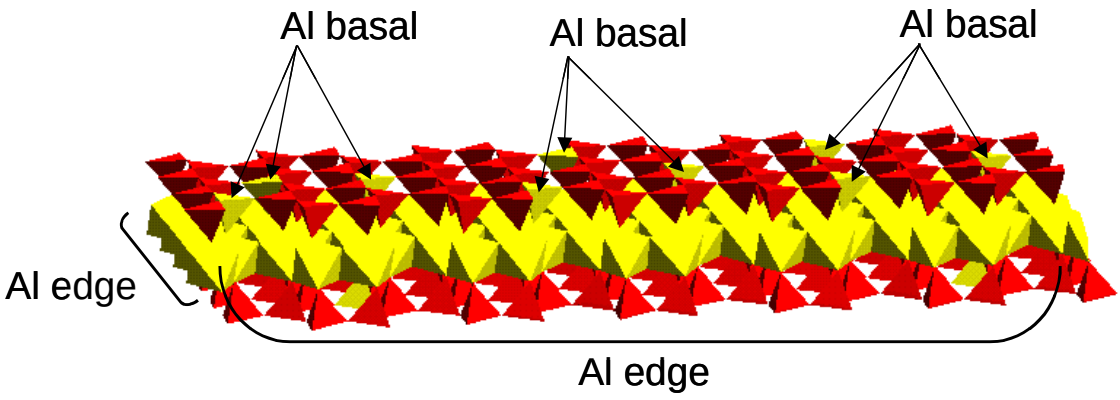

	Basal Plane	**Edge**
Surface Area	90 m^2/g	10 m^2/g
Site Density	0.23 sites/nm^2	2.3 sites/nm^2

Surface Species	**Log *K* of Formation**	
	Basal	**Edge**
$>AlOH_2^+$	-8.33*	-8.33*
$>AlO^-$	1.00	9.73*
$>AlOUO_2^+$	-4.00	-2.70*

*From Pabalan *et al.* (1998)

Figure 1. Aluminum surface sites on a platelet of clay mineral. Two types of Al surface-sites (basal plane tetrahedral Al sites and octahedral Al edge sites) are present. The surface areas and site densities assumed for both the basal plane and edge of smectite are provided for comparison. In addition, the adsorption constants for both the basal and edge surface species are tabulated. The selection of values for these parameters is discussed further in the text.

conditions (Zhang et al., 2001). In this model, only two surface complexes with uranium are considered, $>(e)AlOUO_2^+$ and $>(b)AlOUO_2^+$, where uranium adsorbs to the edge (*e*) and basal (*b*) surface sites, respectively. Each of these complexes forms according to the following type of reaction:

$$>(e)AlOH + UO_2^{2+} \leftrightarrow >(e)AlOUO_2^+ + H^+;$$

$$K = \frac{m_{>(e)AlOUO_2^+} a_{H^+}}{m_{>(e)AlOH} a_{UO_2^{2+}}} 10^{(+F\Psi / 2.303RT)} \quad (8)$$

Other types of uranyl surface complexes may be present on clay surfaces in the subsurface environment. In particular, uranyl carbonate and uranyl bicarbonate surface complexes are expected to play an important role in uranium attenuation in carbonated groundwater (e.g., Waite et al., 1994; Thompson et al., 1998). In addition, several different types of uranyl complexes may be adsorbed onto the clay surface at any given time. However, in order to investigate the sensitivity of calculated uranium migration to uncertainties in adsorption constant values used, the model was limited to including only two uranyl surface complexes, $>(e)AlOUO_2^+$ and $>(b)AlOUO_2^+$. The variability of the *K* given in equation (8) was examined for the formation of $>(e)AlOUO_2^+$.

Following Pabalan et al. (1998), the optimal (mean) acidity constants for surface protonation and deprotonation on the Al edge sites are assumed to be equivalent to those for corundum (Turner and Sassman, 1996). The optimal uranyl adsorption constant for the Al edge sites is also taken to be equivalent to that for Al edge sites on montmorillonite (Pabalan et al., 1998). For the Al basal sites, the protonation constant was set equal to that for the edge sites because surface protonation is unlikely to occur over the pH range represented in the simulations. The equilibrium constant for deprotonation [$>(b)AlO^-$] was assigned a low value to ensure that basal sites remain deprotonated over the pH range (i.e., pH 5.8 to 8.0) considered in the simulations. Adsorption on the basal sites is independent of pH and is ascribed to the negative charge associated with the substitution of aluminum for silicon in the tetrahedral sheet. For uranyl adsorption to the basal planes, the equilibrium constant was selected such that adsorption is much less than onto the edge sites, but large enough to provide a non-zero baseline for uranium adsorption plots.

4. ONE-DIMENSIONAL SIMULATIONS

To examine the influence of adsorption constant values on the conceptual geochemical models, the study focused on a series of 1-D simulations. First, the effect of grid spacing on the numerical solution is discussed. Next, the uncertainty associated with adsorption constants and their influences on transport is considered. The 1-D system considered here consists of a 500 m long domain. While the upstream boundary was subject to a discharge rate of 20 m/yr, the downstream boundary is assumed to be open. The aquifer is initially contaminated (see the groundwater compositions in Table 2), where uniform aquifer porosity and permeability of 0.3 and 3.12×10^{-13} m^2 respectively were used throughout the domain. Finally, the longitudinal dispersivity was chosen to be 5 m. Simulations were performed to model times up to 20 years.

4.1 Effect of Grid Spacing on Numerical Solution

Figure 2 illustrates breakthrough curves for uranium in fluid over a five year period, using grid spacings Δx of 5, 2.5, and 1.25 m where the concentration has been normalized to C/C_0. Here, C is the uranium concentration in ppm and C_o is the initial concentration in the contaminated groundwater in ppm. The continuous influx of rainwater dilutes the contaminated groundwater such that, after approximately

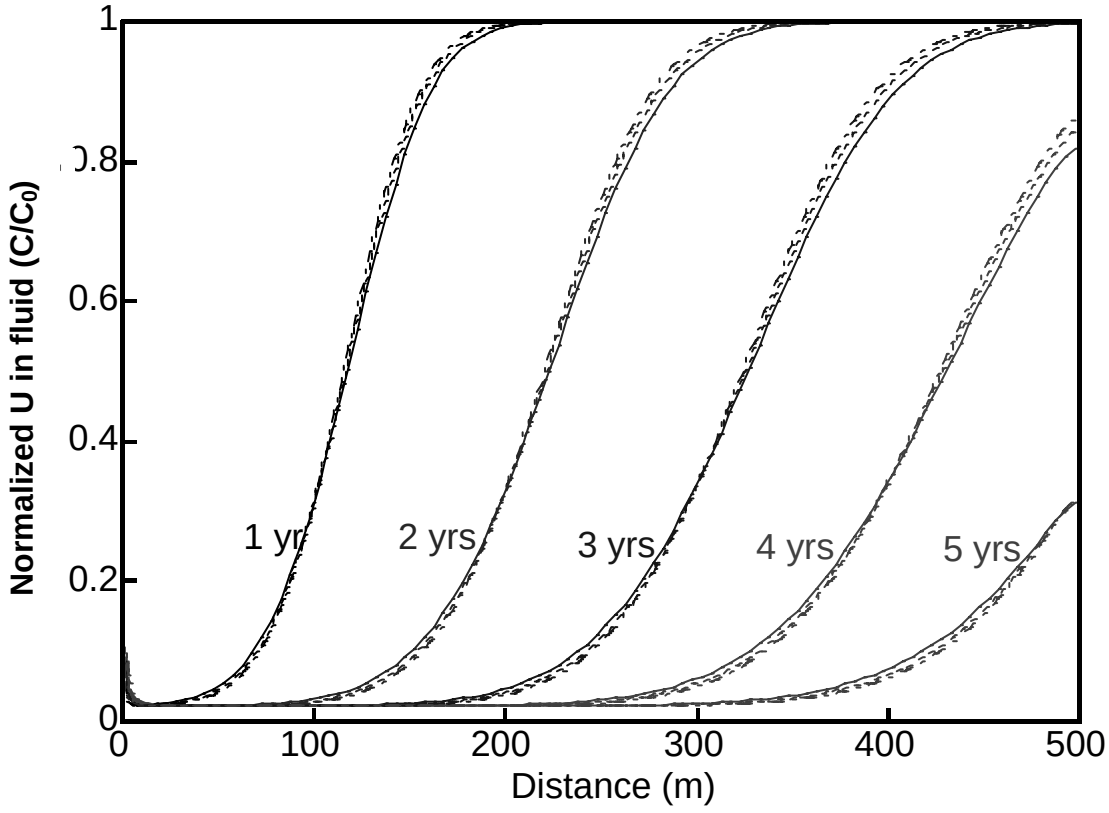

Figure 2. Effect of grid spacing on uranium in fluid profiles as a function of time, using X1t geochemical simulator. The uranium concentration in solution, *C*, is normalized by the initial concentration of uranium, C_o, in the contaminated groundwater. The normalized concentration profiles illustrate that there is little sensitivity to the choice of grid spacing. Here, solid, dashed, and dash-dot lines refer to a grid spacing of 5, 2.5, and 1.25 m, respectively, where all simulations are performed using the mean log *K* values for >(e)AlO^- and >(e)$AlOUO_2^+$.

four years at a distance of about 380 m, the normalized concentration is reduced by over 50%. More importantly, however, the uranium concentration profiles are similar for all three Δx values. This suggests that for the system considered here, the numerical solution is relatively insensitive to the choice of grid spacing. Therefore, the grid spacing was allowed to be 5 m in subsequent 1-D simulations in order to efficiently use the computational resources. Note that, for Δx=5 m, the grid Peclet number (i.e., $P_e=\Delta x/\alpha_L$) is equal to one, which is well within the customary constraint of $P_e \leq 2$ (e.g., see Frind and Germain, 1986).

4.2 Uncertainty Analysis: Latin Hypercube Sampling

Uranyl adsorption is expected to be predominantly a function of the equilibrium constants for $>(e)AlOUO_2^+$ and $>(e)AlO^-$ (Pabalan et al., 1998). For this reason, the uncertainty in these two constants was investigated. The range of equilibrium constant values was chosen to be comparable to the range of surface protonation and deprotonation constants found by Hayes et al. (1991) who, using the DLM, fitted surface titration data for goethite, corundum, and rutile using total surface site densities of 1, 10, and 100 sites/nm^2. Fitted (de)protonation constants varied by over three log units to compensate for the variance in site density. The study by Hayes et al. (1991) remains the only investigation that thoroughly examined variable sensitivity within the DLM. Accordingly, for the sensitivity analysis, we varied the equilibrium constants for $>(e)AlOUO_2^+$ and $>(e)AlO^-$ were varied approximately over three orders of magnitude.

To analyze the influences of adsorption constants on the numerical reactive-transport results, the Latin Hypercube Sampling (LHS) technique was used to generate normally distributed pairs of log *K* values. Unlike simple Monte Carlo approaches where samples are randomly generated, LHS employs a constrained sampling scheme (e.g., Iman and Shortencarier, 1984). On the basis of equal probability, the LHS technique generally divides the range of each variable (e.g., two log *K*s in this case) into *n* nonoverlapping intervals. For a given probability density function (e.g., normal distribution), one random value from each interval is then selected. Subsequently, the *n* values obtained for one variable are paired with *n* values for the other variable, thus forming the *n* pairs of random values. Figure 3 presents 100 pairs of normally distributed log *K*s for $>(e)AlO^-$ and $>(e)AlOUO_2^+$, generated using the LHS software package developed by Wyss and Jorgensen (1998). Here, the mean log *K* values for $>(e)AlO^-$ and $>(e)AlOUO_2^+$ are respectively chosen to be 9.73 and –2.7, and a $\Delta\log K = 1.5$ is used to represent two standard deviations from the mean log *K*. In the next section, the consequences of the log *K* variations (i.e., uncertainty) on our 1-D conceptual model are discussed.

4.3 Results

The log K $>(e)AlO^-$ and log K $>(e)AlOUO_2^+$ variations for the 100 simulations yield different adsorbed uranium concentrations, as well as different distributions of aqueous species, for the initial conditions of each transport simulation. The total uranium concentration in the system is 1200 ppm. Using the mean log *K* values for both surface species, the equilibrium concentration of uranium in solution is 3.14 ppm, well within the range observed at the Naturita site. For the 100 pairs of log *K* values used in the simulations, the initial uranium in solution varies from 2.47×10^{-4} ppm to 1053.0 ppm. As Figs. 4a and 4b illustrate, while this initial aqueous uranium concentration is a strong function of log K $>(e)AlOUO_2^+$, it is less dependent upon the choice of log K $>(e)AlO^-$.

The range of initial uranium concentrations in solution is significant, particularly considering that the maximum concentration level (MCL) is 0.03 ppm (USEPA, 2001). In order to analyze differences in breakthrough curve behavior, the results of each simulation were normalized to the initial uranium concentration in aqueous solution (C_o) for that simulation. The results can be generally divided into two main groups: Group A, in which the calculated breakthrough curves exhibit a uniform concentration front (e.g., similar to those seen in Fig. 2), and Group B, in which the breakthrough curves exhibit a sharp spike in uranium concentration at the inlet followed by an undulation in uranium concentration with distance. Representative breakthrough curves for these two different types of response are illustrated in Figs. 5a and 5b for various simulation times. Note that while the calculated breakthrough curves represent the amount of uranium in solution, they fail to emphasize that the majority of the uranium present in the system often remains adsorbed onto the clay throughout the simulation. For example, for log K $>(e)AlO^-$ = 11.71 and log K $>(e)AlOUO_2^+$ = -3.92, the initial

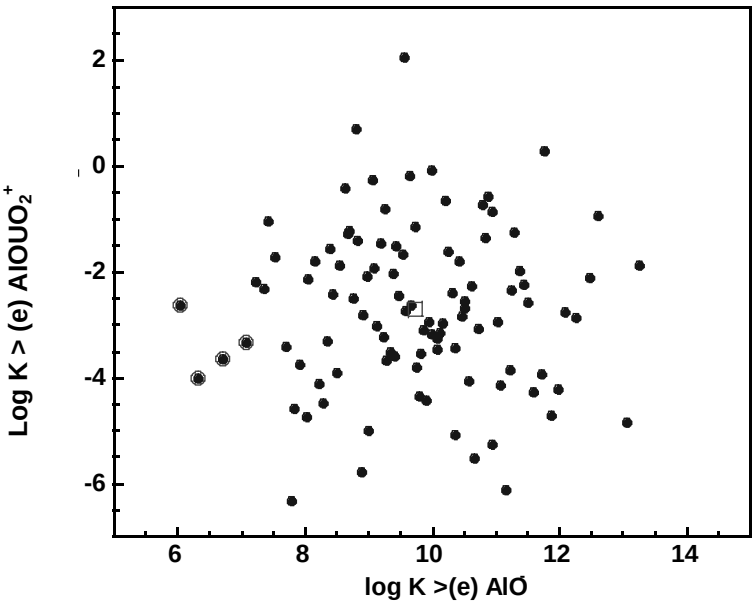

Figure 3. Log *K* variation for >(e) $AlOUO_2^+$ versus those of >(e) AlO^- for 100 pairs of values generated using Latin Hypercube Sampling technique. The 100 samples, indicated with solid dots, are based on a normal distribution with two standard deviations from the mean log *K*. The value for the mean log *K* pair is shown with an open square, and the open circles around four of the 100 samples indicate the simulations that failed to run.

equilibrium distribution of uranium is 0.11 mg/kg uranium in solution and over 1055 mg/kg uranium adsorbed. After two years of simulated time, the uranium in solution drops to below 0.01 mg/kg near the inlet while the uranium adsorbed remains between 1054 and 1056 mg/kg throughout the 1-D domain. On the other hand, in some simulations, the uranium present is more equally distributed between the solution and the smectite surface; for example, for log K $>(e)AlO^-$ = 9.72 and log K $>(e)AlOUO_2^+$ = -1.14, the initial uranium concentrations are 560 mg/kg in solution and 490 mg/kg adsorbed.

Figure 6 illustrates the simulated breakthrough curves, after two years of rainwater infiltration into the system, for 96 different pairs of log K values (as indicated in Fig. 3, four out of the 100 simulations failed to run). These breakthrough curves can again be clearly separated into two groups: Group A, in which the breakthrough occurs approximately 200 m downstream from the inlet, and Group B, in which breakthrough generally occurs fairly close to the inlet boundary. Interestingly enough, the same two-group responses can also be seen over all simulation times. For instance, Fig. 7 depicts the breakthough curves, as a function of time, at the downstream boundary. While one can clearly distinguish the two groups, C/C_0 for most of Group A cases is less than 0.2 while there is generally a decreasing trend in the uranium concentration for Group B. However, for a number of simulations, C/C_0 reduces to approximately 0.7 after about 6 years, after which it either remains unchanged or displays a slight increasing trend (see the five uppermost curves in Fig. 7).

Because there are clearly two different breakthrough curve behaviors exhibited by Groups A and B, it was decided to check the effect of grid spacing on the numerical solution of a Group B simulation in the same way that its effect on the breakthrough curves calculated using the optimum (mean) log Ks (see Section 4.1, Fig. 2) was analyzed. Using grid spacings Δx of 5, 2.5, and 1.25 m, the breakthrough curves for the Group B simulation were found to be insensitive to grid spacing for five-year simulations.

Referring back to Fig. 4a, it is clear that these two groups separate according to the log K $>(e)AlO^-$: The majority of breakthrough curves in Group A are from simulations in which the log K $>(e)AlO^-$ values range from 7 to 10, while those in Group B result from simulations in which the log K $>(e)AlO^-$ values range

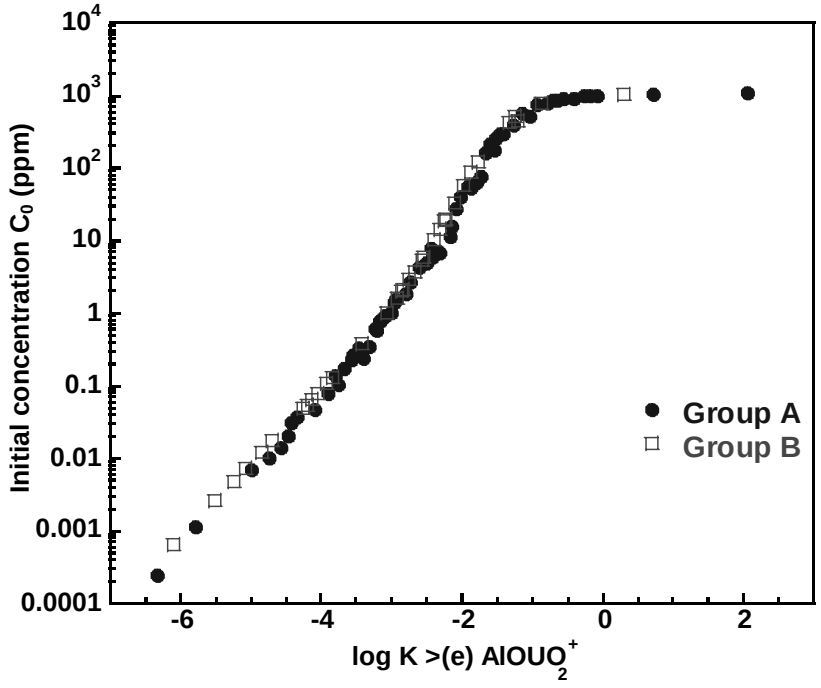

4a

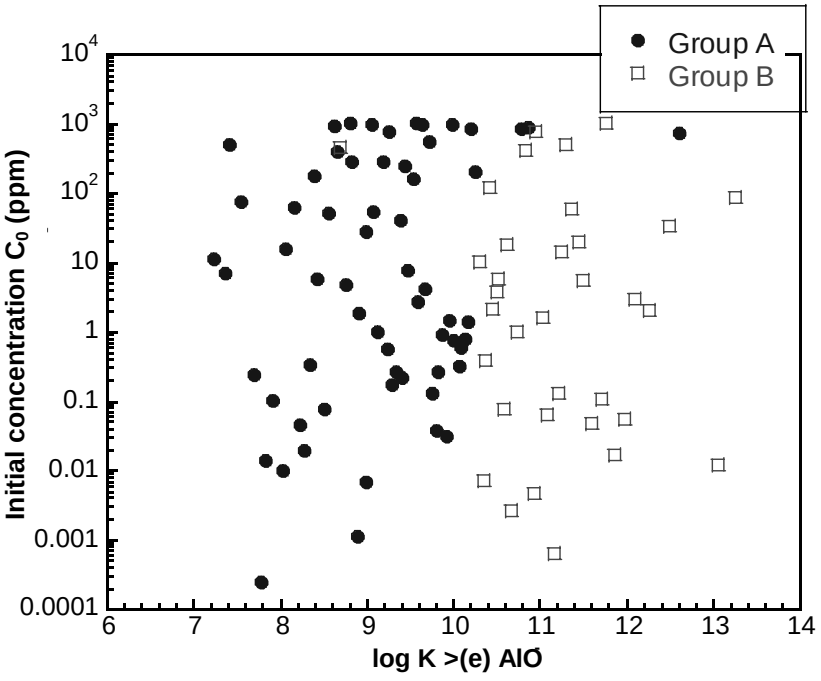

4b

Figure 4. Initial concentration values for uranium in fluid versus (a) log *K* >(e) $AlOUO_2^+$ and (b) log *K* >(e) AlO^-. The concentrations are divided into two groups, A and B, because the 100 pairs of log *K* values sampled and illustrated in Fig. 3 lead to two distinctly different types of breakthrough curve behavior (see Fig. 6).

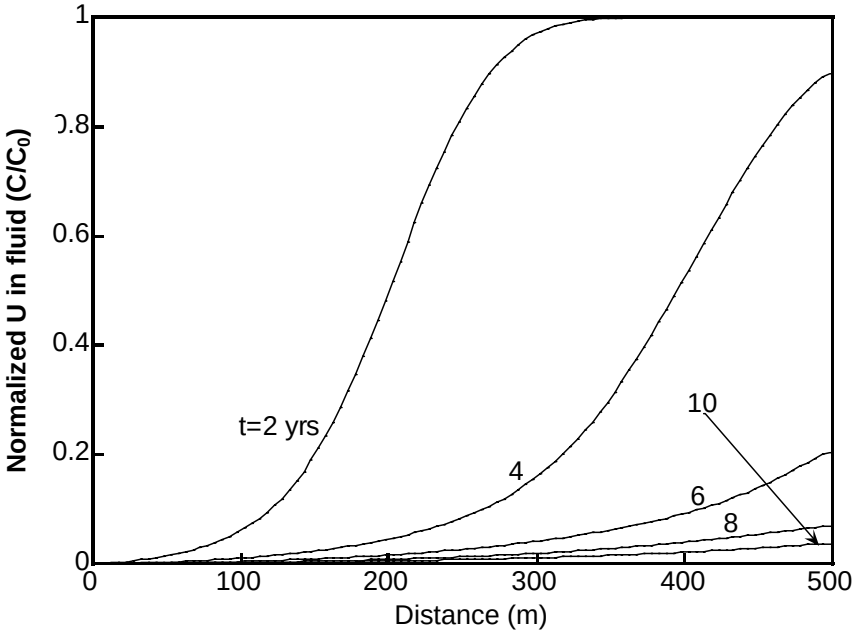

5a

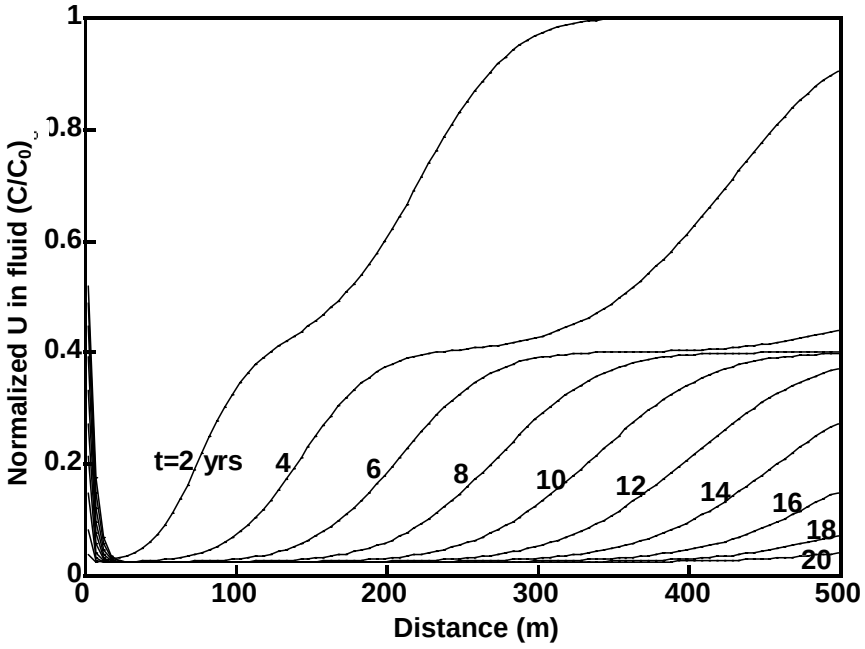

5b

Figure 5. Temporal development of concentration profiles for aqueous uranium typical of (a) Group A and (b) Group B results. For Group B, a combination of geochemical factors leads to smectite dissolution at the inlet releasing a spike in uranium concentration and resulting in a secondary wave of uranium release into the groundwater.

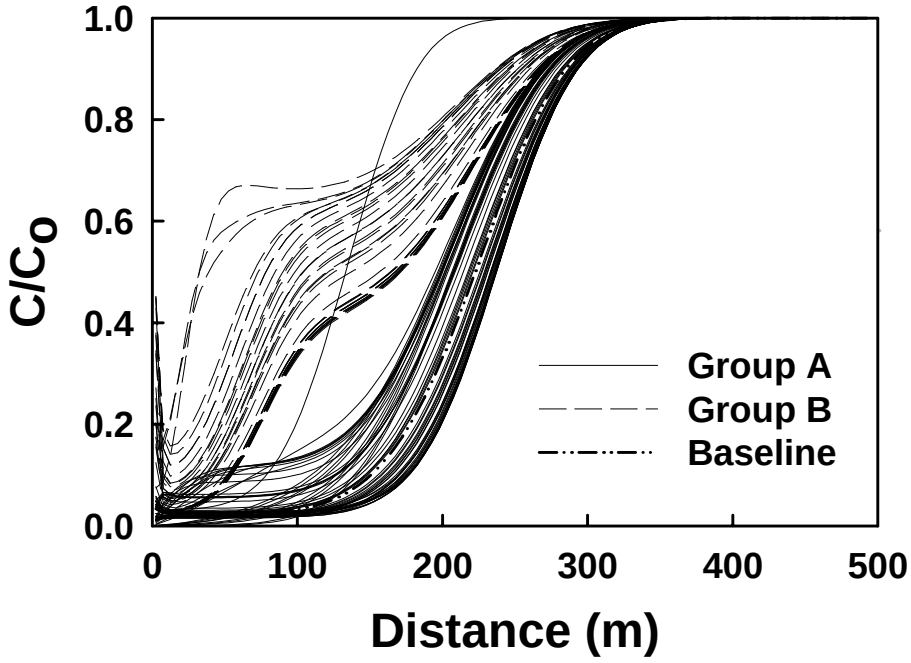

Figure 6. Normalized concentration profiles of uranium in fluid versus distance, after 2 years, for 96 out of the 100 LHS realizations. The various curves clearly show that the simulated results fall into two categories indicated as Groups A and B. The profile for the baseline case (i.e., using mean log *K* values) is also indicated.

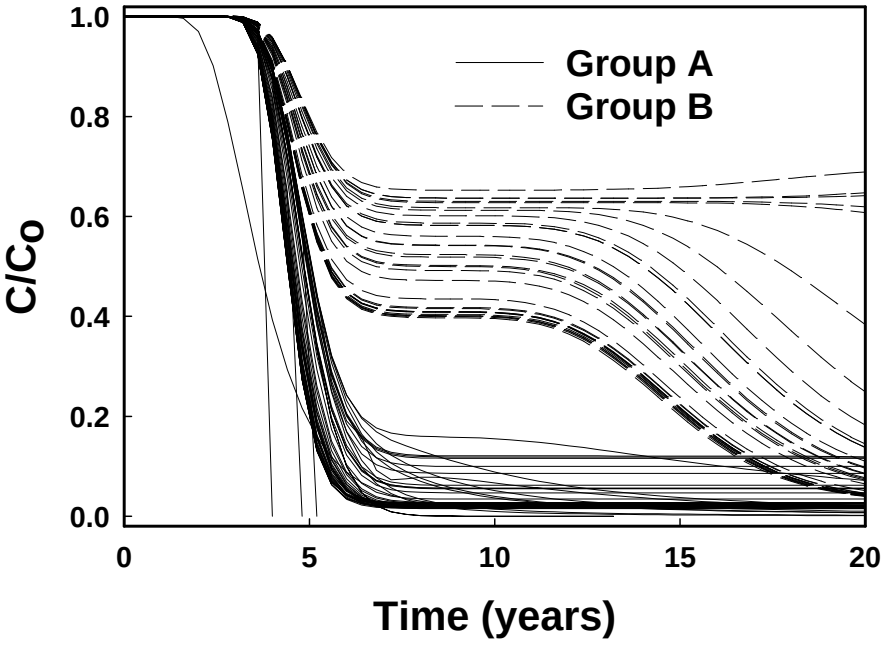

Figure 7. Breakthrough curves at the downstream boundary, illustrating the variations of the normalized uranium concentration as a function of time, for the profiles in Fig. 6. As in Fig. 6, the same two-group behaviors persist throughout all simulations. The curves that abruptly drop after approximately 3 to 5 years indicate several simulations that did not run to completion (i.e., 20 years).

from 10.5 to 13.5. These two groups cannot be distinguished by the log K $>(e)AlOUO_2^+$. High and low initial concentrations of uranium are present in both Groups A and B. This observation is also supported by plots of the breakthrough distances measured from the inlet to the center of the breakthrough curve (i.e., at 50% uranium in solution) after two years of mixing, shown in Fig. 8. Again, the two groups demonstrate a marked dependence on the log K $>(e)AlO^-$.

These results suggest that surface protonation may be critical in determining the shape and rate of migration of uranium breakthrough curves. The concentration of H^+ adsorbed to smectite will affect the groundwater pH. From examining the simulation results, it becomes evident that there are other influences on the pH of the groundwater. For example, the precipitation and dissolution of low-Fe-Mg smectite strongly affects the groundwater pH. In both Groups A and B, the pH of the solution near the inlet increases over time, sometimes to values higher than that of the initial groundwater (e.g., pH 8). As rainwater and groundwater mix, a small fraction of smectite dissolves. This dissolution consumes H^+ (see equation (6)) that causes an increase in pH. In addition, the mixing of solutions with different $f\mathrm{CO}_2(g)$ influences the ratio of HCO_3^-, CO_3^{2-} and $CO_2(aq)$, as well as the relative concentrations of metal-carbonate complexes present in solution.

The aqueous complexation of both aluminum and uranium is very sensitive to pH over the range of values covered in the simulations (pH 5.8 to 8.0). While only two uranyl surface complexes are included, these complexes might actually form from any of the aqueous uranyl species available. For example, many different reactions might contribute to the adsorption of uranyl to the smectite surface, including:

$$>(e)AlOH + UO_2^{2+} \leftrightarrow >(e)AlOUO_2^+ + H^+ \qquad (9a)$$

$$>(e)AlOH \;+\; UO_2(CO_3)_2^{2-} + H^+ \leftrightarrow >(e)AlOUO_2^+ + 2HCO_3^- \qquad (9b)$$

$$2>(e)AlOH \;+\; (UO_2)_2(CO_3)(OH)_3^- + 2H^+ \leftrightarrow 2>(e)AlOUO_2^+ + HCO_3^- \;+\; 2H_2O. \qquad (9c)$$

Reactions between uranyl carbonate or uranyl hydroxide species in solution and the surface to form uranyl surface complexes will also modify the pH of the solution. In general, the uranium initially dissolved in the contaminated groundwater is present predominantly as negatively charged or neutral uranyl carbonate and hydroxide complexes. With the addition of rainwater, positively charged uranyl hydroxide complexes become the predominant aqueous uranyl species, and both uranyl-sulfate and hydrous uranyl-silica complexes become more important in the overall uranyl speciation scheme. The exact distribution of aqueous uranyl species is a function of the log K values chosen for $>(e)AlO^-$ and $>(e)AlOUO_2^+$.

The breakthrough curves exhibited by Group A using this complex geochemistry are similar in shape to breakthrough curves calculated using a constant distribution coefficient or K_d model. By selecting the inflection point of a Group A breakthrough curve after simulating two years of transport and reaction, a K_d value was estimated and was subsequently used to model uranium adsorption for comparison with the surface complexation model. To implement a K_d model in the X1t code, the K_d is defined as the number of moles of adsorbed species (UO_2^{2+}) per gram of solid (smectite) divided by the activity of the free ion (UO_2^{2+}) in solution. A comparison between the breakthrough curves described by the K_d model and the surface complexation model is provided in Fig. 9 after two and four years of simulated time. It is apparent that the curves calculated using the two models differ in shape and location over time due to the difference in adsorption models. It should be pointed out that in the K_d model implemented here, complete aqueous geochemical speciation is still included, which includes more reaction chemistry than is frequently considered in more simplistic reactive-transport models.

Because all of the reactions described above occur for both Groups A and B, an important question is exactly why there is such an apparent distinction between the two groups. The log K $>(e)AlO^-$ ranges from 7 to 10 for Group A and 10.5 to 13 for Group B, while the log K $>(e)AlOUO_2^+$ remains constant at -8.33. Therefore, the pH of the pristine point of zero charge (pH_{ppzc}), or the pH at which protonated and deprotonated sites achieve charge balance for the Al edge sites, varies from 7.66 to 9.16 for Group A and 9.42 to 10.66 for Group B. For both groups, the smectite surface is positively charged; however, the smectite surfaces will be more positively charged for

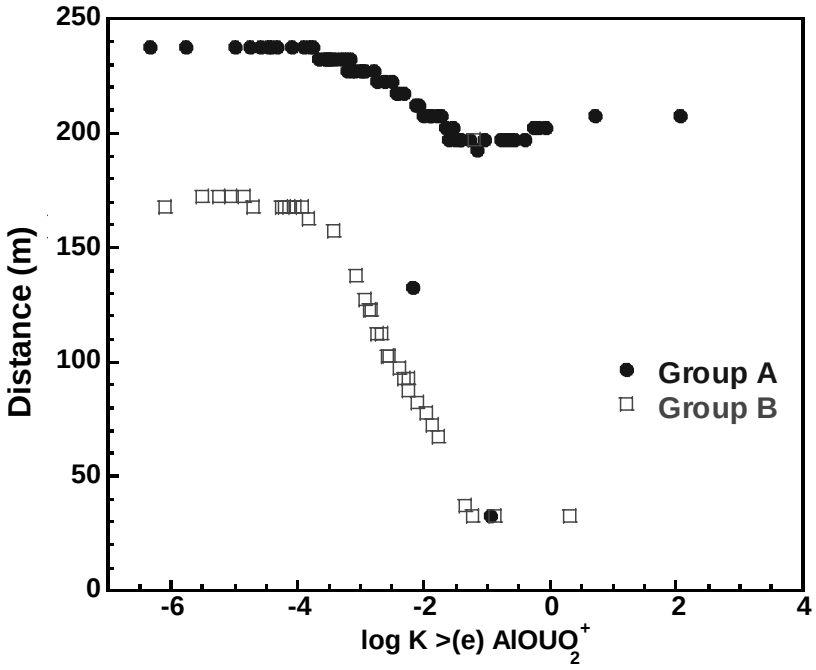

8a

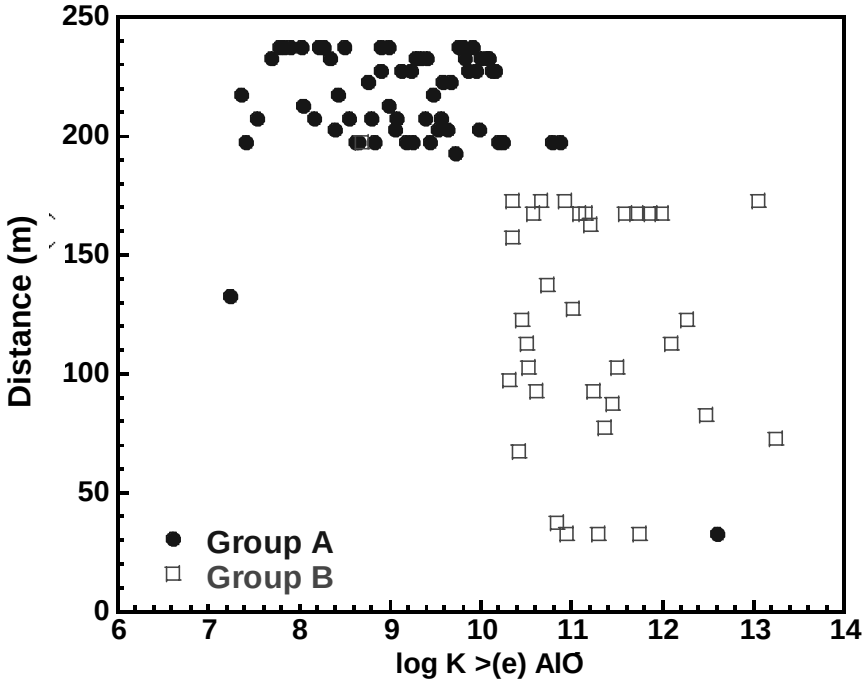

8b

Figure 8. Breakthrough distance representing a C/C_0~0.5 of uranium in fluid versus (a) log K >(e) $AlOUO_2^+$ and (b) log K >(e) AlO^-. The various simulations are separated based on the two observed groups A and B.

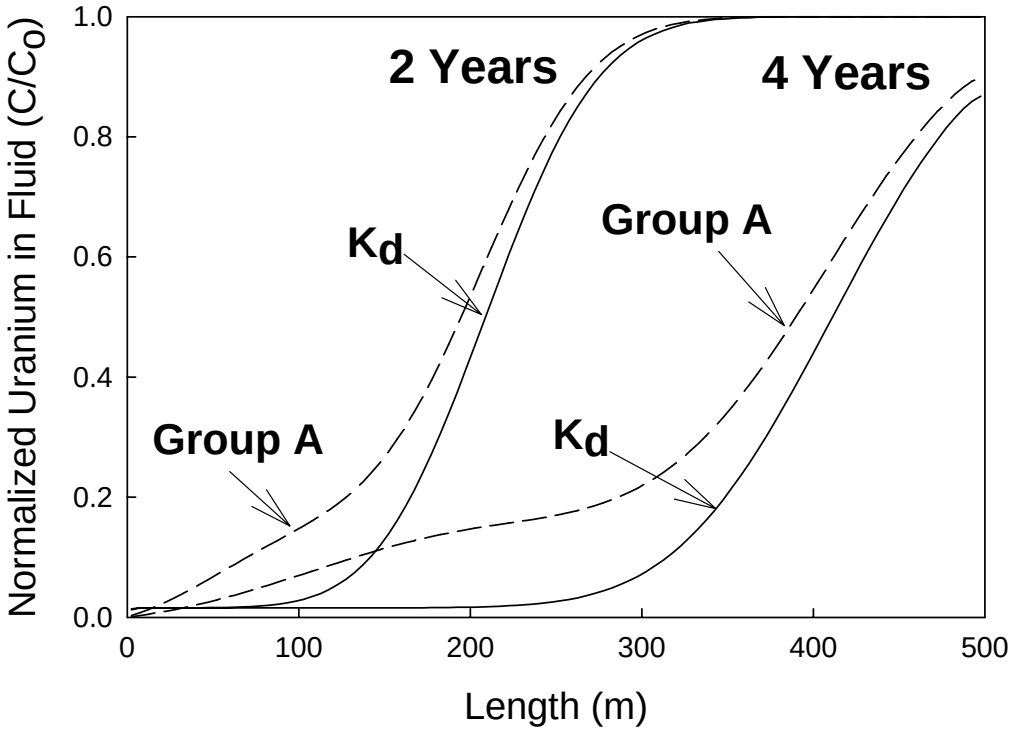

Figure 9. Comparison of normalized uranium in fluid with distance for a simulation from Group A and a comparable K_d model after 2 and 4 years of simulated time. Initial equilibrated aqueous uranium concentrations are 560 mg/kg for the Group A case and 1,050 mg/kg for the K_d case, although the total uranium contents are equivalent. The K_d breakthrough curves are more sigmoidal and symmetric than those calculated using the DLM.

Group B, in which the pH range covered in the simulations is more pH units away from the pH_{ppzc} than in Group A. This distinction between Groups A and B provides a strong hint of how the fundamental surface charge controls uranyl adsorption.

Because of the complexity of the reactive transport system, several simpler and controlled simulations were performed to determine the parameters involved in creating the unusual shape of the Group B breakthrough curves. The inlet fluid was first modified until it closely resembled the contaminated groundwater that is in equilibrium with smectite. The mixing of the two fluids results in an instability in smectite equilibrium, which propagates downstream as the dissolution and reprecipitation of smectite. This fluctuation in smectite stability releases uranium into solution so that a pulse of increasing uranium in the groundwater grows with time and distance downstream. This pulse is accompanied by a spiked increase in bicarbonate and carbonate species in solution. The pH of the system fluctuates sympathetically with smectite dissolution and precipitation. In simulations in which the influent fluid is modified by changing the fCO_2 and the pH to match that of rainwater, the system parameters exhibit the same general behavior. The fluctuations in smectite stability and pH values, and the spikes in aqueous uranium and carbonate species, are not observed in identical simulations using adsorption constants from Group A.

The undulatory shape of Group B breakthrough curves is reproduced when the electrolyte concentrations (Na^+, Ca^{2+}, Cl^-, and SO_4^{2-}) in the inlet fluid are returned to values found in rainwater. This shape is therefore, in part, the result of mixing two fluids of differing electrolyte concentrations and ionic strengths. The ionic strength of the solution influences the surface charge and potential of the diffuse layer model (DLM) through the Gouy-Chapman equation that describes the relationship between surface charge and potential. This equation reduces to (Dzombak and Morel, 1990):

$$\sigma = 2.5 I^{1/2} \Psi \qquad (10)$$

for water at 25°C, where σ [C/m^2] is the surface charge density, I [mol/L] is the ionic strength, and Ψ [V] is the surface potential.

The difference in ionic strength between the rainwater (10^{-4} M) and the contaminated groundwater (>10^{-2} M) will affect the thickness of the diffuse layer of the DLM. Surface protonation increases nonlinearly as a function of ionic strength and pH on the positive side of the zero point of charge. The smectite surface sites defined by Group B adsorption constants will exhibit more dramatic variation in protonation state than the surface sites defined by Group A adsorption constants. The differences in electrolyte concentrations will also influence the aqueous speciation schemes for uranyl, as well as for all of the other cations and anions in solution.

In conclusion, the variation in values for adsorption constants for >(*e*)AlO^- and >(*e*)$AlOUO_2^{2+}$ examined in this study affects the overall stability of smectite as well as the surface properties of the clay. As a consequence, calculations of uranyl migration are strongly affected by these perturbations and will lead to significant variations in the calculated breakthrough curves.

5. ILLUSTRATIVE TWO-DIMENSIONAL SIMULATIONS

To determine the effects of the variation of adsorption constant values on the temporal variations in uranium plume geometry, a series of preliminary simulations based on a 2-D conceptual model were initiated. The 2-D areal region consisted of a 500 m long by 200 m wide domain to represent the near-field environment of the Naturita site. For this system, the longitudinal and transverse dispersivity values were set to α_L=5 m and α_T=0.5 m. The groundwater and the water discharged into the domain (i.e., the inlet boundary condition) were assumed to be initially free of uranium and have a composition similar to that of uncontaminated groundwater at the Naturita site (see Table 2). While groundwater discharge rate (i.e., the Darcy flux) at the inlet boundary was assumed to be 20 m/yr, leachate (see Table 2 for composition) was introduced through an injection well at a rate of 20 m^3/day. The well was located 50 m downstream from the inlet boundary and 100 m from the lower boundary of the domain. In addition, to explore the influence of subsurface heterogeneity, the aquifer porosity, ϕ, was described using a normal distribution with a mean and standard deviation of 0.25 and 5%, respectively. Note that within the context of the X2t model, the underlying intrinsic permeability, k, varies according to $k=9.87 \times 10^{(-18+15\phi)}$ m^2. For the 2-D simulations described below, a uniform grid spacing with $\Delta x=\Delta y$=10 m was used, where Δy represents the grid spacing in the transverse direction.

Figure 10 depicts the uranium plume geometries for two different pairs of log K values selected to represent the general behavior of the two groups, A and B, derived from the 1-D simulations. In a 20-year period, the uranium plume described by Group A adsorption constants migrates further downstream and spreads more widely in the transverse direction than that of the uranium plume calculated using adsorption constants from Group B. These results are not in obvious agreement with the conclusions from the 1-D simulations. However, the breakthrough curves in the 1-D simulations effectively represent uranyl desorption from smectite, while the uranium plumes depicted in the 2-D simulations reflect the influence of uranyl adsorption. In addition, the fluid compositions in the 1-D simulations differ in fCO_2 and pH, and differ more greatly in electrolyte concentrations than the fluid compositions used in the 2-D simulations. Combined, these differences will influence the concentration of adsorbed uranyl.

The shapes of the contaminant plumes illustrated in Fig. 10 are not dramatically different from each other, nor significantly different from the shapes of contaminant plumes described by K_d models. However, it is clear from the 1-D simulations that, although a single snapshot of a contaminant migration simulation can be adequately mimicked by a K_d model, the time and distance evolution of a plume will be described very differently using a surface complexation model.

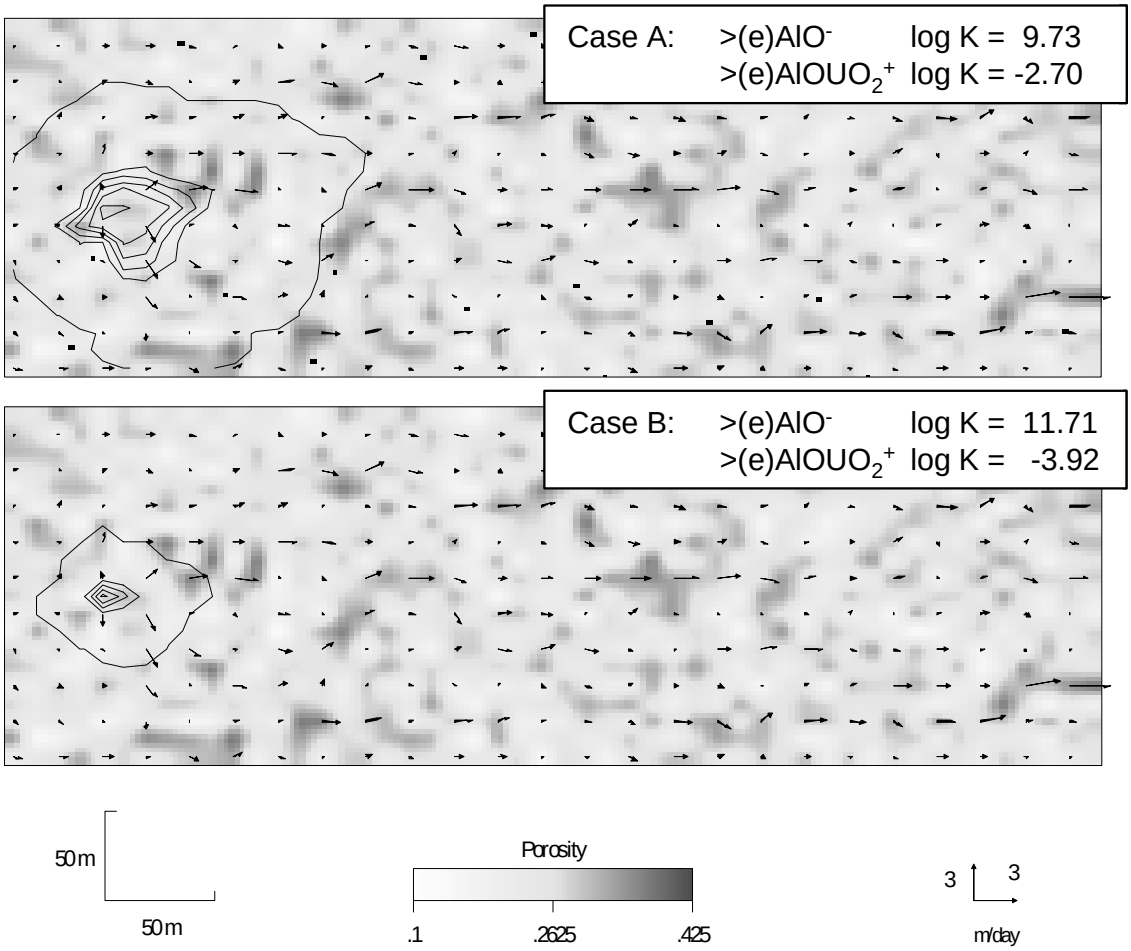

Figure 10. Map view of the results of 20 years of reactive transport of uranium obtained from two representative situations (Case A and Case B realizations) based on the variation in the thermodynamic values for the critical sorption parameters. The outermost contour for each plot represents a background level of 1×10^{-6} ppm of uranium in the groundwater, with a contour interval of 0.5 ppm up to 2.5 ppm at the innermost contour. Variation in porosity, generated by a normal distribution about a mean 0.25 porosity value with a 5% standard deviation, is represented by the gray shading. Groundwater velocity arrows are presented at every other nodal point of the simulation grid.

6. CONCLUSIONS

This probabilistic investigation demonstrates that the uncertainty in two thermodynamic values for describing adsorption in complex natural systems, using 1- and 2-D reactive-transport models, can dramatically change the shape of contaminant breakthrough curves in 1-D and contaminant plumes in 2-D. For the 100 pairs of log K values selected for the simulations, the initial uranium concentration in solution varies over seven orders of magnitude, from approximately 0.0001 to 1000 ppm. In the 1-D simulations, two different groups of breakthrough curves, A and B, can readily be distinguished. In Group A, the breakthrough curves exhibit a classical sigmoidal shape. In Group B, the breakthrough curves display greater changes in aqueous uranium concentration (C/C_o) over smaller distances and times than in Group A. These two groups of breakthrough curves differ because of the values chosen for log $K >(e)AlO^-$ (i.e., 7 to 10 for Group A and 10.5 to 13 for Group B). Variations in the value of log $K >(e)AlO^-$ effectively change the point of zero charge for the smectite and the influence of electrostatics in uranyl adsorption. In addition, the shape of the Group B breakthrough curves are influenced by smectite dissolution at the inlet and variations in ionic strength due to the mixing of dilute rainwater and uranium mill-tailings leachate.

In the 2-D simulations, the spread of the uranyl plume in both the vertical and transverse directions is influenced by variations in the adsorption constants. These results suggest that further investigation into the effects of adsorption constant uncertainty on plume shape and size is warranted. A more detailed examination of the fraction of uranium adsorbed from both the 1-D and 2-D simulations will provide a link between the 1-D and 2-D results.

Page intentionally left blank.

7. REFERENCES

Anderson, G. M. (1976) "Error propagation by the Monte Carlo method in geochemical calculations." *Geochimica et Cosmochimica Acta* **40**: 1533-1538.

Bear, J., and A. Verruijt (1987) *Modeling Groundwater Flow and Pollution.* D. Reidel, Norwell, Mass.

Bain, J. G., K. U. Mayer, D. W. Blowes, E. O. Frind, J. W. H. Molson, R. Kahnt, U. Jenk (2001) "Modelling the closure-related geochemical evolution of groundwater at a former uranium mine." *Journal of Contaminant Hydrology* **52**: 109-135.

Bethke, C. M. (1996) *Geochemical Reaction Modeling: Concepts and Applications.* Oxford University Press, New York, 397 pp.

Bethke, C. M. (1997a) *Xt Model of Transport in Reacting Geochemical Systems, Notes to Accompany the Xt Modeling Workbook.* Hydrogeology Program, University of Illinois, Urbana-Champaign.

Bethke, C. M. (1997b) "Modelling transport in reacting geochemical systems." *Comptes Rendus de l'Académie des Sciences: Sciences de la Terre et des Planètes* **324**: 513-528.

Bethke, C. M. (1998) *The Geochemist's Workbench: A User's Guide to Rxn, Act2, Tact, React and Gtplot. Release 3.0.* Craig M. Bethke, University of Illinois, 184 pp.

Berner, E. K. and R. A. Berner (1996) *Global Environment: Water, Air and Geochemical Cycles.* New Jersey, Prentice Hall, 376 pp.

Brady, P. V., R. T. Cygan and K. L. Nagy. (1998). "Surface charge and metal sorption to kaolinite." In *Adsorption of Metals by Geomedia: Variables, Mechanisms, and Model Applications.* Edited by E. A. Jenne. New York, Academic Press**:** 371-382.

Criscenti, L. J., G. F. Laniak, and R. L. Erikson. (1996) "Propagation of Uncertainty through Geochemical Code Calculations." *Geochimica Cosmochimica Acta* **60**, 3551-3568.

Curtis, G. P., J. A. Davis, M. Kohler, and D. M. Meece (2002) "Comparison of adsorption models in reactive transport simulations of U(VI) under conditions of spatially variable alkalinity." *Water Resources Research*, in press.

Curtis, G. P., J. A. Davis, M. Kohler, and D. M. Meece (2001). "Reactive transport modeling of U(VI) in groundwater at a former mill site." (abstract) In *Eleventh Annual V. M. Goldschmidt Conference.* LPI Contribution No. 1088, Lunar and Planetary Institute, Houston (CD-ROM).

Cygan, R. T., K. L. Nagy, and P. V. Brady (1998) "Molecular models of cesium sorption on kaolinite." In *Adsorption of Metals by Geomedia: Variables, Mechanisms, and Model Applications.* Edited by E. A. Jenne. New York, Academic Press**:** 383-399.

Davis, J.A. (2001) *Surface complexation modeling of uranium(VI) adsorption on natural assemblages.* NUREG/CR-6708, Nuclear Regulatory Commission (NRC), Washington, D.C.

Davis, J. A. and D. B. Kent (1990) "Surface complexation modeling in aqueous geochemistry." *Mineral-Water Interface Geochemistry.* Edited by M. F. Hochella, Jr. and A. R. White. Washington, D. C., Mineralogical Society of America. **23:** 177-260.

Davis, J. A., M. Kohler, D. M. Meece, C. Sanpawanitchakit, D. B. Kent, G. P. Curtis, and B. D. Honeyman (2001). "Application of semi-empirical surface complexation models to metal and radionuclide transport." (abstract) In *Eleventh Annual V. M. Goldschmidt Conference.* LPI Contribution No. 1088, Lunar and Planetary Institute, Houston (CD-ROM).

Davis, J. A. and J. O. Leckie (1978) "Surface ionization and complexation at the oxide/water interface II. Surface properties of amorphous iron oxyhydroxide and adsorption of metal ions." *Journal of Colloid and Interface Science* **67**: 90-107.

Davis, J. A., R. O. James, and J.O. Leckie (1978) "Surface ionization and complexation at the oxide/water interface I. Computation of electrical double layer properties in simple electrolytes." *Journal of Colloid and Interface Science* **63**: 480-499.

Domencio, P. A., and F. W. Schwartz (1990) *Physical and Chemical Hydrogeology,* John Wiley and Sons, Inc., New York.

Dzombak, D. A. and F. M. M. Morel (1990) *Surface Complexation Modeling: Hydrous Ferric Oxide.* John Wiley and Sons, New York. 393pp.

Erikson, R. L., C. J. Hostetler, and M. L. Kemnar (1990) *Mobilization and Transport of Uranium at Uranium Mill Tailings Disposal Sites.* NUREG/CR-5169 PNL-7154, Nuclear Regulatory Commission (NRC), Washington, D. C.

Frind, E. O., and D. Germain (1986) "Simulation of contaminant plumes with large dispersive contrast: Evaluation of alternating direction Galerkin models." *Water Resources Research* **22**: 1857-1873.

Gelhar L. W. (1986) "Stochastic subsurface hydrology from theory to applications." *Water Resources Research* **22**: 135S-145S.

Hayes, K. F., G. Redden, W. Ela, and J. O. Leckie (1991) "Surface complexation models: An evaluation of model parameter estimation using FITEQL and oxide mineral titration data." *Journal of Colloid and Interface Science* **142**, 448-469.

Hamed, M. M., P. B. Bedient, and J. P. Conte (1996). "Numerical stochastic analysis of groundwater contaminant transport and plume containment." *Journal of Contaminant Hydrology* **24**: 1-24.

Iman, R. L. and M. J. Shortencarier (1984) *A Fortran 77 Program and User's Guide for the Generation of Latin Hypercube and Random Samples for Use with Computer Models.* NUREG/CR-3624, Technical Report SAND83-2365, Sandia National Laboratories, Albuquerque, NM.

Jacobs Engineering Group Inc. (1994) *UMTRA Project Water Sampling and Analysis Plan: Naturita, Colorado.* DOE/AL/62350-121F, Department of Energy (DOE) – Grand Junction Office (GJO): Grand Junction, CO.

Jové Colón, C. F., P. V. Brady, M. D. Siegel, and R. Lindgren (2001). "Historical Case Analysis of Uranium Plume Attenuation." *Soil and Sediment Contamination* **10**: 71-115.

Jové Colón, C. F., C. Sanpawanitchakit, H. Xu, R. T. Cygan, J. A. Davis, and D. M. Meece (2002) A Combined Analytical Study to Characterize Uranium Soil Contamination: The Case of the Naturita UMTRA Site and the Role of Grain Coatings. Nuclear Regulatory Commission (NRC), Washington, D.C. (in press)

Kohler, M., D. M. Meece, and J. A. Davis (2001) A comparison of methods for estimating sorbed uranium(VI) in contaminated sediments. (abstract) In *Eleventh Annual V. M. Goldschmidt Conference*. LPI Contribution No. 1088, Lunar and Planetary Institute, Houston (CD-ROM).

Landa, E. R. and J. R. Gray (1995) "U.S. Geological Survey – Research on the environmental fate of uranium mining and millings wastes." *Environmental Geology* **26**: 19-31.

Morrison, S. J. and L. S. Cahn (1991) "Mineralogical residence of alpha-emitting contamination and implications for mobilization from uranium mill tailings." *Journal of Contaminant Hydrology* **8**: 1-21.

Nordstrom, D. K. and J. W. Ball (1989) "Mineral saturation states in natural waters and their sensitivity to thermodynamic and analytical errors." *Sciences Geologique Bulletin*, **42**: 269-280.

Nitzsche, O., G. Meinrath, and B. Merkel (2000) "Database uncertainty as a limiting factor in reactive transport prognosis." *Journal of Contaminant Hydrology* **44**: 223-237.

Neuman, S. P. (1990) "Universal scaling of hydraulic conductivities and dispersivities in geologic media." *Water Resources Research* **26**: 1749-1758.

Pabalan, R. T., D. R. Turner, F. P. Bertetti, and J. D. Prikryl (1998) "Uranium^{VI} sorption onto selected mineral surfaces: Key geochemical parameters." In *Adsorption of Metals by Geomedia: Variables, Mechanisms, and Model Applications.* Edited by E. A. Jenne. New York, Academic Press: 99-130.

Schecher, W. D. and C. J. Driscoll (1987) "An evaluation of uncertainty associated with aluminum equilibrium constants." *Water Resources Research* **23**, 525-534.

Schecher, W. D. and C. J. Driscoll (1988) "An evaluation of the equilibrium calculations within acidification models: the effect of uncertainty in measured chemical components." *Water Resources Research* **24**, 533-540.

Schlegel, M. L., L. Charlet and A. Manceau (1999). "Sorption of Metal Ions on Clay Minerals II. Mechanism of Co Sorption on Hectorite at High and Low Ionic Strength and Impact on the Sorbent Stability." *Journal of Colloid and Interface Science* **220**: 392-405.

Stipp, S. L. (1990) "Speciation in the Fe(II)-Fe(III)-SO_4-H_2O System at 25°C and Low pH: Sensitivity of an Equilibrium Model to Uncertainties." *Environmental Science and Technology* **24**: 699-706.

Tebes-Stevens, C. L., F. Espinoza, and A. J. Valocchi (2001) "Evaluating the sensitivity of a subsurface multicomponent reactive transport model with respect to transport and reaction parameters." *Journal of Contaminant Hydrology* **52**: 3-27.

Tebes-Stevens, C. L. and A. J. Valocchi (2000) "Calculation of reaction parameter sensitivity coefficients in multicomponent subsurface transport models." *Advances in Water Resources* **23**: 591-611.

Thompson, H. A., G. A. Parks, and G. E. Brown Jr. (1998) "Structure and composition of Uranium^{VI} sorption complexes at the kaolinite-water interface." In *Adsorption of Metals by Geomedia: Variables, Mechanisms, and Model Applications.* Edited by E. A. Jenne. New York, Academic Press**:** 349-370.

Turner, D. R. and S. A. Sassman (1996) "Approaches to sorption modeling for high-level waste performance assessment." *Journal of Contaminant Hydrology* **21**: 311-332.

USEPA (2001) *National Primary Drinking Water Standards.* EPA-816-F-01-003, United States Environmental Protection Agency, Office of Water (4606), Washington, D.C.

Waite, T. D., J. A. Davis, T. E. Payne, G. A. Waychunas, and N. Xu (1994) "Uranium (VI) adsorption to ferrihydrite: Application of a surface complexation model." *Geochimica et Cosmochimica Acta* **58**: 5465-5478.

Wyss, G. D, and K. H. Jorgensen (1998) *A User's Guide to LHS: Sandia's Latin Hypercube Sampling Software.* Technical Report SAND98-0210, UC-505, Sandia National Laboratories, Albuquerque, NM.

Zachara, J. M. and J. P. McKinley (1993) "Influence of hydrolysis on the sorption of metal cations by smectites: Importance of edge coordination reactions." *Aquatic Sciences* **55**: 250-261.

Zhang, P. C., P. V. Brady, S. E. Arthur, W. Q. Zhou, D. Sawyer, D. A. Hesterberg (2001) "Adsorption of barium(II) on montmorillonite: an EXAFS study." *Colloids and Surfaces A- Physicochemical and Engineering Aspects* **190**: 239-249.

Zhu, C. and D. S. Burden (2001) "Mineralogical compositions of aquifer matrix as necessary initial conditions in reactive contaminant transport models." *Journal of Contaminant Hydrology* **51**: 145-161.

Zhu, C., F. Q. Hu, D. S. Burden (2001) "Multicomponent reactive transport modeling of natural attenuation of an acid groundwater plume at a uranium mill tailings site." *Journal of Contaminant Hydrology* **52**: 85-108.

Page intentionally left blank.